#3931

Experimental Study of Three-Dimensional Natural Convection High-Rayleigh Number

M. S. Bohn
Solar Energy Research Institute,
Golden, Colo. 80401
Assoc. Mem. ASME

A. T. Kirkpatrick
Mechanical Engineering Department,
Colorado State University,
Ft. Collins, Colo.
Assoc. Mem. ASME

D. A. Olson
Mechanical Engineering Department,
Massachusetts Institute of Technology,
Cambridge, Mass.
Assoc. Mem. ASME

Natural convection in buildings is characterized by three-dimensional flow at high Rayleigh numbers ($Ra \sim 10^{10}$). At present, little is known about natural convection heat transfer in this regime, although a better understanding would allow more energy efficient usage of buildings. This paper presents results from the first phase of an experimental program aimed at improving our understanding of heat transfer and air flow in buildings. The experimental apparatus consists of a cubical enclosure filled with water in which each wall may be heated or cooled in a controlled manner. A transparent, adiabatic top and bottom provide flow visualization capability. Average heat transfer coefficients for the walls have been measured for several configurations of heating and cooling of the vertical isothermal walls. A unified Nu-Ra correlation has been computed which collapses the heat transfer coefficients of the various configurations to within 5.7 percent. The heat transfer and flow visualization results indicate that even at Rayleigh numbers as high as 6×10^{10}, the heat transfer mechanism is laminar boundary-layer convection from one wall to the bulk fluid.

Introduction

In this paper, we address the problem of three-dimensional natural convection in enclosures with differentially heated vertical walls at high Rayleigh numbers. The particular application of interest is passive solar heating and cooling of buildings, although the experimental data should be useful in many other applications as well. These include cryogenic storage tanks, building fires, nuclear reactor cooling, and solar cavity receivers. In addition, the data should be useful in three-dimensional numerical code validation and in determining the validity of the assumption of two-dimensionality in previous experiments.

The objective of the research is to determine the natural convection flow patterns and heat transfer coefficients between heated and cooled vertical walls in a cubical enclosure. This problem involves three-dimensional flow between perpendicular walls, as well as across parallel walls.

Natural convection heat transfer across fluid-filled enclosures has been the subject of many analytical, numerical, and experimental investigations. The flow regimes in the two-dimensional problem involving heat transfer between two parallel walls were first delineated by Batchelor [1] using a Rayleigh number criterion, and subsequently confirmed by Eckert and Carlson [2]. At Rayleigh numbers greater than 10^4 and aspect ratios near 1, the laminar boundary layer regime exists. The heat transfer mechanism is convection in boundary layers along the vertical walls surrounding a core region. The core region is relatively inactive, is isothermal in the horizontal direction, and has a linear temperature gradient in the vertical direction. Elder [3, 4] and Gill [5], for A, aspect ratios >1, where the aspect ratio is the ratio of enclosure height to length, have shown there is entrainment between the hot and cold wall boundary layers, due to the top and bottom surfaces of the enclosure, resulting in stable thermal stratification of the core. In addition, their results show that the boundary layer heat transfer is only weakly dependent on the Prandtl number of the fluid in the enclosure.

As the Rayleigh number is increased, the thickness of the velocity and temperature boundary layers decreases, since the boundary layer thicknesses are proportional to $A^{1/4}\ Ra^{-1/4}$. Bejan [6] has extended Gill's laminar boundary layer solution for $A > 1$ to predict heat transfer rates. The resulting equation, valid as $A\ Ra^{1/7} \to \infty$ is $Nu = 0.364\ A^{-1/4}\ Ra^{1/4}$. Simpkins and Dudderar [7] have experimentally checked Gill's boundary layer analysis for $0.25 < A < 9$. An approximate boundary layer analysis for aspect ratios > 5 was performed by Raithby et al. [8, 9], and an integral boundary layer analysis has been performed by Emery and Chu [10]. For a fluid with a Prandtl number of 3.5, the Raithby-Hollands analysis predicts $Nu = 0.335 A^{-1/4}\ Ra^{1/4}$. In summary, the previous boundary layer analyses for $A > 1$ predict $Nu = (.3 \text{ to } .4)\ A^{-1/4}\ Ra^{1/4}$. For turbulent flow, the Raithby-Hollands analysis predicts $Nu = 0.044\ Ra^{1/3}$. The two foregoing predictions are plotted in Fig. 1 for $A = 1$.

Numerical results for aspect ratios between 1 and 20, and Grashof number $< 10^5$ have been presented by Newell and

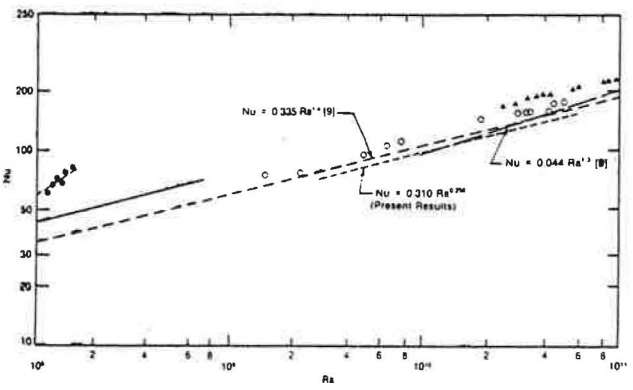

Fig. 1 Compilation of two-dimensional high Rayleigh number data and comparison with present results

- – – – Raithby-Hollands laminar boundary layer theory (9), $A = 1$, $Pr = 3.5$
- – – Raithby-Hollands turbulent boundary layer theory (9), $A = 1$, $Pr = 3.5$
- ——— Gadgil numerical analysis (23), $A = 1$, $Pr = 0.7$
- ○ Bauman et al. (27), $A \doteq 0.5$, $Pr = 3.5$
- ▲ Nansteel and Greif (29), $A = 0.5$, $Pr = 3.5$
- ● Burnay et al. (18), $A = 1$, $Pr = 0.7$

Contributed by the Heat Transfer Division and presented at the ASME-JSME Joint Thermal Engineering Conference, Honolulu, Hawaii, March 1983. Manuscript received by the Heat Transfer Division May 2, 1983.

Schmidt [11] for aspect ratios between 0.1 and 20, by Boyack and Kearney [12] and aspect ratios between 0.05 and 1, and $Ra < 10^6$ by Inaba et al. [13]. Numerical results for $Ra < 10^7$ and aspect ratios of 1, 5, and 10 have been computed by Strada and Heinrich [14]. The numerical results predict a maximum Nusselt number near an aspect ratio of one, and as the aspect ratio approaches zero or infinity, the Nusselt number approaches unity, a trend also noted by Bejan [15]. Also, as the Rayleigh number is increased, the aspect ratio at which the maximum Nusselt number occurs decreases. In Inaba's [13] numerical analysis, the aspect ratio at which the Nusselt number was a maximum decreased from $A = 1.7$ at $Ra = 10^4$ to $A = 1.2$ at $Ra = 10^5$. Bejan [15] predicted that the maximum Nusselt number would occur at $A = 0.4$ for $Ra = 10^6$; $A = 0.25$ to $Ra = 10^7$; and $A = 0.18$ at $Ra = 10^8$. The data (from an experiment with $A = 0.5$) plotted on Fig. 1 follow the same trend, since they lie above the $A = 1$ predictions.

Limited two-dimensional experimental data exist for $Ra > 10^8$ and A near 1. MacGregor and Emery [16] found experimentally for constant heat flux conditions and aspect ratios from 10 to 40 that $Nu = 0.42 A^{-0.3} Pr^{0.012} Ra^{1/4}$ for $3 \times 10^4 < Ra < 3 \times 10^6$ and $Nu = 0.046 Ra^{1/3}$ for $3 \times 10^7 < Ra < 10^9$. For the aspect ratios of their experiment, they determined that the transition from fully laminar to fully turbulent boundary layer flow occurred in the range of Rayleigh numbers from 3×10^6 to 3×10^7. Dropkin and Sommerscales [17] reported experimental results for Rayleigh numbers from 5×10^4 to 7.2×10^8. Experimental data for air in a square enclosure with Rayleigh numbers from 1.2×10^8 to 1.7×10^8 have been presented by Burnay et al. [18]; however, the precision of their results is suspect since the correction for radiation heat transfer was of the same magnitude as the natural convection heat transfer. Measurements and correlation equations have been published by ElSherbiny et al. [19] for $A \geq 5$, and Rayleigh numbers from 10^2 to 2×10^7.

Increased attention has been focused recently on natural convection heat transfer in rectangular cavities with aspect ratios less than one. Bejan and Tien [20] have predicted that for $0.1 < A < 1$, $Nu = 0.623 A^{-2/5} Ra^{1/5}$. Shiralkar et al. [21] analytically and numerically show that for laminar flow and $A < 1$, as $Ra \to \infty$, $Nu \to 0.354 Ra^{1/4}$. The exponent of the Rayleigh number was shown to be not constant, but a decreasing function of Rayleigh number. Analytical and numerical calculations were performed by Tichy and Gadgil [22] for $A = 0.1$, 0.2, and $Ra > 10^6$. Numerical results have been reported by Gadgil [23] for $A = 1$ and $10^4 < Ra < 10^9$, and are plotted in Fig. 1.

Imberger [24] found experimentally that as $Ra \to \infty$, $Nu \to A Ra^{1/4}$ for $A = 0.01$, 0.02. Bejan et al. [25] reported that $Nu = 0.014 Ra^{0.38}$ for $A = 0.0625$ and $2 \times 10^8 < Ra < 2 \times 10^9$. Experimental results for the flow pattern in enclosures with aspect ratios between 0.1 and 10 have been reported by Sernas and Lee [26]. Experiments with a water filled cavity with $A = 0.5$ an Prandtl number variation from 2.6 to 6.8 have been reported by Bauman et al. [27], Gadgil et al. [28], and Nansteel and Greif [29] for Rayleigh numbers from 1.6×10^9 to 1.1×10^{11}. The data points from [27] and [29] are plotted in Fig. 1.

There are very few articles in the literature on three-dimensional flow in enclosures with differential side heating. Mallinson and deVahl Davis [30] numerically solved for the laminar temperature and velocity fields in a cubical enclosure with adiabatic endwalls. The endwalls induced a double spiral motion in the core, and decreased the average Nusselt number by about 3 percent relative to a two-dimensional case. The endwall effect decreased with increasing Rayleigh number, from a 4.8 percent difference at $Ra = 10^4$ to a 2.6 percent difference at $Ra = 10^6$. This small effect shows that in the laminar boundary layer regime, the overall heat transfer is not very sensitive to the flow pattern in the core region. As the endwalls are moved from an endwall aspect ratio of 1 to 5, the endwall effect on the Nusselt number decreases from 4.2 percent to 2.3 percent at a constant Rayleigh number of 1.5×10^5. A numerical study of three-dimensional turbulent flow in a ventilated room was performed by Hjertager and Magnussen [31]. Gadgil [23] numerically calculated a hot wall average Nusselt number of 145 for a cube with one of its vertical surfaces maintained at a uniformly higher temperature than the other five surfaces at $Ra = 1.15 \times 10^{10}$. Morrison and Tran [32] measured the effect of endwall conduction on the velocity and temperature profiles for $A = 5$, and $Ra = 5 \times 10^4$. A literature search did not reveal any results for perpendicular vertical walls.

Description of the Experiment

The test cell, Fig. 2, is a cubical enclosure, interior dimension 30.5 cm, constructed of eight 1.27-cm-thick aluminum plates. The four inner plates overlap one another and are screwed together with a neoprene gasket to form the enclosure. The four outer plates provide heating and cooling to the four enclosure walls as shown in Fig. 3. The outer plates are sealed and bolted to the inner plates.

Three of the walls have a centered thermocouple located to within 3 mm of the enclosure inner surface. The fourth wall has eight such thermocouples. These thermocouples are located on a horizontal line 5 cm above and 5 cm below the wall center and spaced on 5 cm centers from the wall vertical centerline. The wall thermocouples (copper-constantan) indicate the average wall temperature and spatial variation of the wall temperature across the plate. The spatial variation was less than 10 percent (typically 5 percent) of the overall

Nomenclature

A = aspect ratio, height to length ratio of a two-dimensional enclosure
A_w = area of enclosure wall (cm^2)
g = acceleration of gravity (cm/s^2)
H = height of a two-dimensional enclosure (cm)
h = average heat transfer coefficient of enclosure wall $= Q/A_w \lvert T_w - T_b \rvert$ ($W/cm^2 °C$)
k = thermal conductivity of test cell fluid ($W/cm °C$)
L = plate spacing of cubical enclosure (cm)
m = exponent of Ra (−)
Nu = Nusselt number $= hL/k$ (−)
Pr = Prandtl number of test cell fluid (−).
Q = heat transferred to or from wall (W)
Ra = Rayleigh number $= g\beta\Delta TL^3 Pr/\nu^2$ (−)
T = temperature (°C)

Subscript

b = bulk
c = cooled wall
h = heated wall
H = based on height dimension
x = based on distance from leading edge
w = wall

Greek Symbols

β = coefficient of thermal expansion ($°C^{-1}$)
ΔT_o = overall temperature difference $= T_h - T_c$ (°C)
ν = kinematic viscosity

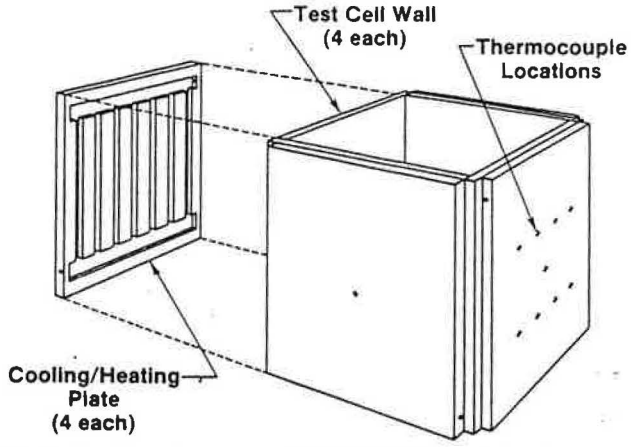

Fig. 2 Diagram of the cubical enclosure test cell. Interior dimensions of the cube are 30.5 cm.

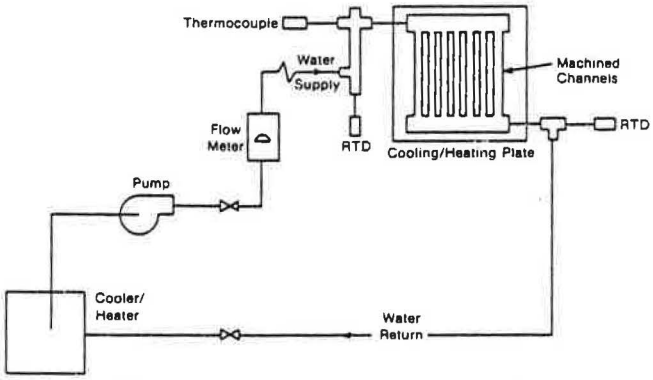

Fig. 3 Diagram of the cooling/heating circuits

temperature difference, $T_h - T_c$. Therefore, the heated and cooled walls may be considered isothermal.

For flow visualization purposes, the top and bottom of the enclosure consists of 1.27-cm-thick lucite plates screwed to the top surface of the inner plates with a neoprene gasket. The top plate has four compression fittings with rubber septums that allow hypodermic tubing to be inserted into the test cell. Diluted food coloring is used as the dye and injected through the hypodermic tubing into the test cell. The dye is injected through a micrometering valve for flow control at approximately 5 cc per hour flow rate. Total volume of injected dye for a typical 1-hr experiment from all four dye ports is therefore about 0.8 percent of the cell volume. Dye velocity at the tip of the needle is less than 3 mm/s, which is much less than flow velocity in the boundary layers and roughly the same as the core velocities. When the probe is inserted more than 10 cm into the cell, heat transfer from the dye, as it flowed through the needle to the test cell, appeared to bring the dye to thermal equilibrium with the test cell water. For insertions of less than 10 cm, the buoyant effect on the dye could be seen as it exited the tip of the needle. Under these conditions, the dye drifted upward (or downward in warm regions) for about 1 cm before appearing to move with the local flow. When dye was injected into the boundary layer, the probe was adjusted to approach the wall obliquely to create minimum flow disturbance, see Fig. 6. Although this method of flow visualization is far from ideal, it does offer many advantages and is very simple to implement.

The four aluminum test cell walls are insulated with urethane foam board insulation 8.3 cm thick, thermal resistance 4.6°C m^2/W. Heat loss from these four walls is estimated to be about 0.1 percent of the total heat transferred from the walls. The estimate is based on the wall temperature, the outer surface temperature of the insulation, and the thermal resistance of the insulation. Loss from the lucite top (which was usually not insulated) is estimated to be about 0.5 percent. This estimate was made from the highest temperature on the outer surface of the plate, ambient temperature and an assumed natural convection coefficient of 6 W/m^2 °C. The bottom lucite plate operates near ambient temperature and losses from that plate are estimated to be less than 0.2 percent. Therefore, the test cell top and bottom may be considered adiabatic. Heat transferred from a hot wall to a cold wall through the neoprene insulation is estimated to be about 0.8 percent.

Cooling or heating of the four enclosure walls is accomplished by pumping water through milled channels in the four outer aluminum plates, Fig. 3. Hot water is supplied by a 6-kW in-line electric heater, and a domestic hot water tank is used to store and buffer the hot water before it is pumped to the heated enclosure walls. The in-line heater is controlled by a proportional temperature controller that senses the water temperature as it leaves the hot water tank. In this way, water temperature delivered to the heated plates is controlled to within ±1/4°C. Cold water is supplied by pumping the water through a tank that contains a heat exchange coil. By pumping cold tap water through this coil, cold water delivered to the cooled enclosure walls is also controlled to ±1/4°C. A fitting at the channel inlet provides water inlets and outlets and fittings for insertion of a thermocouple in the inlet flow, an RTD probe in the inlet flow and a second RTD in either the inlet or outlet flow. This arrangement is used to measure the change in cooling or heating water temperature in the four walls. The RTD probes are placed in opposite arms of a Wheatstone bridge in such a way that the nominal probe resistance, 100 ohm, is cancelled and a bridge output voltage proportional to the temperature difference measured with this technique was determined by calibration to be ±1 percent for temperature differences greater than about 0.2°C.

Cooling and heating water flow rates, nominally 500 kg/hr, are measured with rotameters. These were calibrated by the stopwatch-and-bucket method to within ±0.5 percent for temperatures near ambient. For the highest temperatures the walls are operated, about 65°C, the flow meters tended to read high by about 2-3 percent, in addition to a decrease of approximately 1.5 percent in the water density (from 30 to 60°C). Partially offsetting those two errors is an error that increases to about 2 percent at 65°C due to nonlinearity of the temperature difference measuring method.

Frictional heating in the cooling/heating channels is responsible for about a 1 percent decrease (increase) in the magnitude of measured heat transfer from (to) the hot (cold) walls. An approximate error analysis based on all four sources of error, suggests that the heat transfer measurement for each wall is accurate to ±2 percent. Data are not corrected for conduction through the neoprene gasket from a hot wall to a cold wall (about 0.8 percent), nor for radiation heat transfer from the hot wall to the cold walls (about 1.6 percent). Overall heat balances in the test cell (total measured heat transfer from hot walls minus total measured heat transfer to the cold walls divided by total measured heat transfer from the hot walls) is typically better than ±2 percent, although for low Rayleigh number tests (less than 0.5×10^{10}) this increased to ±4 percent. Overall heat transfer measurement is expected to be within ±5 percent of the actual convective heat transfer from each wall.

The working fluid in the test cell is de-ionized water. To eliminate the formation of air bubbles in the test cell, the water was brought to a slow boil for two hours, allowed to cool, then poured slowly into the cell. Water used for diluting the food coloring dye is treated similarly. The test cell was carefully leveled with a bubble-type machinists level. Thermal

expansion of the test cell water is accommodated by a small expansion tank held about 20 cm above the test cell and connected by flexible tubing to the cell.

Properties of the water (thermal conductivity, dynamic viscosity, density, coefficient of thermal expansion) in the test cell are calculated at a temperature equal to the average of the four heated/cooled wall temperatures, referred to as the bulk temperature, T_b. Specific heat was taken as constant (4.19 J/gm°C). The length scale used in calculating the Nusselt number and Rayleigh number is L = 30.5 cm and, the area used to derive the heat transfer coefficient is A_w = 930 cm^2. The temperature difference used in deriving the Rayleigh number is the difference in temperatures of the hot and cold walls, i.e., the overall temperature difference.

$$\mathrm{Ra} = \frac{g\beta\Delta T_o L^3}{\nu^2}\,\mathrm{Pr} \tag{1}$$

The temperature difference used to calculate the heat transfer coefficient is the difference between the wall temperature and the bulk temperature

$$\mathrm{Nu} = \frac{hL}{k} \qquad h = \frac{Q}{A_w\,|T_w - T_b|} \tag{2}$$

The four possible different configurations of heated/cooled walls were tested. These are denoted by CHCC, HHCC, HCHC, and HHHC. Here, H refers to a heated wall and C refers to a cooled wall. The wall with eight thermocouples is called wall #1 and is listed first in this scheme. Thus the first series of runs involved wall #1 being cooled, a heated wall adjacent to wall #1, a cooled wall opposite wall #1, and the remaining wall also being cooled.

For each configuration, at least 24 hours is initially allowed to reach steady state. The hot wall temperatures are set to produce several different Rayleigh numbers from 0.3 to 5.0 × 10^{10} with at least 3 hrs allowed to reach steady state between Rayleigh number settings. Steady state is indicated by a steady temperature difference (for constant flow rate) in the heating and cooling water for each wall, i.e., constant wall heat transfer. Generally, the first Rayleigh numbers run are in the middle of the range, then the higher ones are run in increasing order, then Rayleigh numbers decreasing below the first one tested. Results did not vary significantly with the order of testing, however. The Prandtl number varied from about 3.5 to 6 due to variation in the bulk temperature.

At the end of this series of four configurations which spanned a period of about one month, HCCC was run to compare with the first configuration, CHCC. The results for the hot wall for both configurations agreed to within ±5 percent for tests at three Rayleigh numbers ranging from 0.46 to 2.7 × 10^{10}.

Results

Flow visualization experiments confirm the existence of a relatively inactive core region for all configurations. A unique core flow pattern is set up for each configuration. An example is shown in Fig. 4 for the configuration HCHC at Ra = 2.9 × 10^{10}. In Fig. 4, dye is injected at a point about halfway between the top and bottom of the test cell through the port near the top of the photograph. The dye stream moves toward the warm wall, where it apparently splits. A small part of the stream seems to be entrained by the boundary layer as it moves vertically up the wall to approximately 2 cm below the top of the cell. At this point, the dye stream separates from the wall and disperses. The part of the stream moves in a helical pattern, clockwise viewed from above. (A shadow of the upper portion of the helix is projected on the cold wall.) At least one complete rotation of the helix is visible before the dye becomes too diffuse to be clearly seen. Even a portion of the first rotation near the wall is difficult to see. By symmetry, we assume the core flow consists of four such helices with the direction of rotation alternating from corner to corner. Flow velocity was not measured but was estimated by observing the movement of the dye. In the core, the velocity is such that one revolution of the helix in Fig. 4 required several minutes. Velocity in the boundary layers is of the order of 1 cm per s. A repeat of the visualization experiment shown in Fig. 4 for Ra = 0.8 × 10^{10} did not reveal the helical flow in the core. This change in the core flow could be related to a small change in the heat transfer results which will be discussed later in this section.

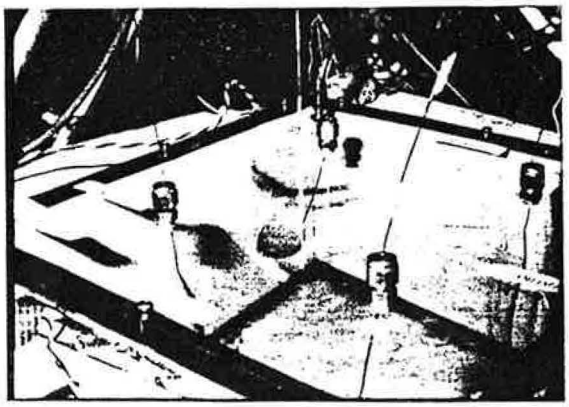

Fig. 4 Flow visualization for the configuration HCHC at Ra = 2.9 × 10^{10}

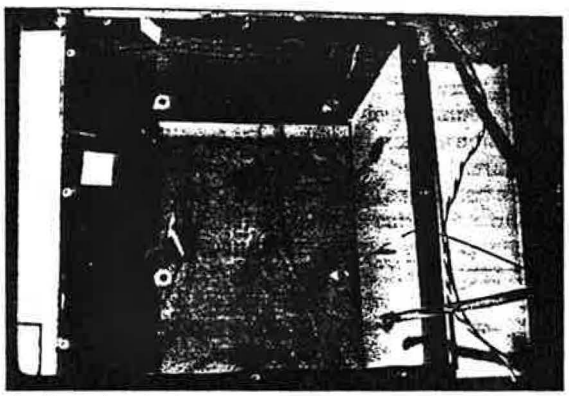

Fig. 5 Flow visualization for the configuration CHCC at Ra = 3.6 × 10^{10}

Figure 5 shows flow visualization results for the configuration CHCC at Ra = 3.6 × 10^{10}. The heated wall is near the top of the photograph. The core flow is depicted by the lower right dye probe, which is inserted to within 3 cm from the cell bottom. The dye stream bends in toward the plane of symmetry and impinges the heated wall normally before being entrained into the boundary layer and flowing upward. From the junction of the wall and the top, the dye proceeds across the top in a similar curved path until it reaches the cooled wall, where it flows downward with the wall boundary layer. Weak cellular structures, not shown in this photograph, were observed in the core near the top center of the two parallel cooled walls. The volume near the intersection of the cooled walls tends to be stagnant.

A cursory examination of the core temperature with copper constantan thermocouples revealed stratification with a nearly linear vertical temperature distribution and weak variations in a horizontal plane, consistent with previous work in two dimensions [1, 2]. The temperature distribution varies from this linear profile near the top and bottom of the cell where heated fluid (top) or cooled fluid (bottom) flowed in a boundary-layer-like flow to the cooled or heated vertical walls.

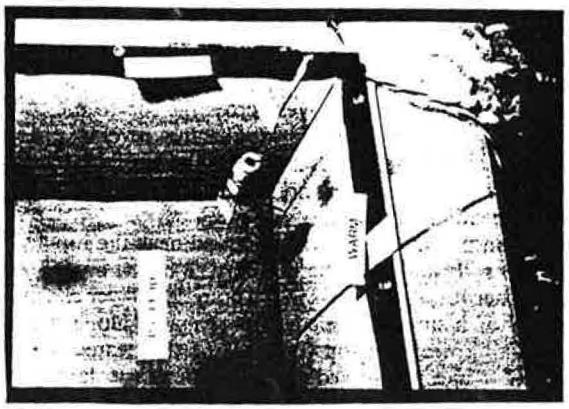

Fig. 6 Flow visualization for the configuration HHCC at Ra = 3.1 × 10^{10}

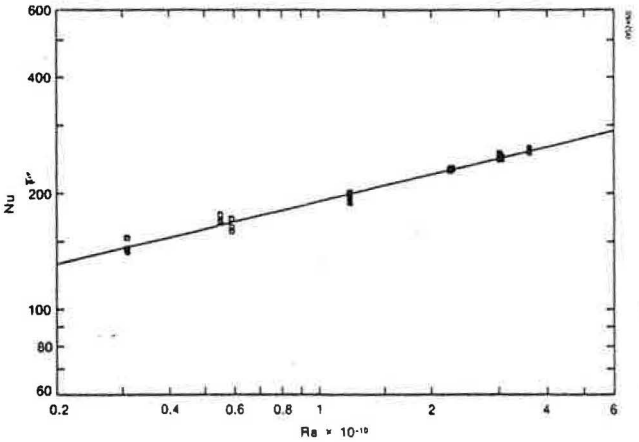

Fig. 7 Heat transfer data for the configuration HHCC

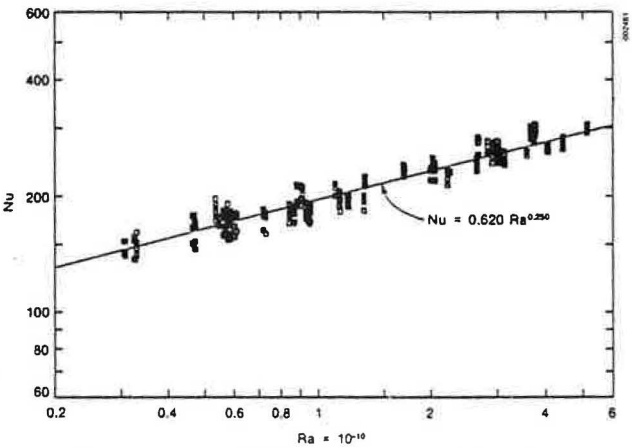

Fig. 8 Heat transfer data for all walls, all configurations

The probe near the top left of the photograph injects dye into the heated wall boundary layer near the bottom of the cell about 1 cm from the cooled wall. As seen in the photograph, the dye stream moves vertically upward and does not appear to be affected by the presence of the nearby cooled wall. The dye stream then moves diagonally across the cell top and vertically down the cooled wall boundary layer about 1 cm from the heated wall.

Also obvious in the photograph is the waviness on the heated wall. The waves are made visible by a shadowgraph effect and represent transition of the heated wall boundary layer. The waves appear to be of a well-defined, single wavelength (about 1 cm) and are essentially two dimensional in nature. The waves appear to break near the top of the test cell. The boundary layer relaminarized after turning the top corner. Similar flow visualization experiments at lower Ra (less than 10^{10}) did not reveal these waves.

The waviness in the boundary layer occurred at local Rayleigh numbers Ra_x, estimated to be between 10^8 and 10^9, where

$$Ra_x = \frac{g\beta(T_w - T_b)x^3}{\nu^2} Pr$$

This result is consistent with the experimental results by Elder [4], who gives the condition for the onset of boundary layer waves as $Ra_x = 3 \times 10^8$ (for aspect ratios between 9 and 27). The linear stability theory calculations of Hieber and Gebhart [33] predict the growth of traveling wave disturbances at Ra_x above 3×10^6 Pr. The difference between the predicted and observed values is due to the vertical distance required for finite amplification of a natural disturbance [34].

Figure 6 also shows waviness, this time towards the bottom of a cooled wall. The probe near the upper right corner of the cell injected dye directly on the wall. The dye stream seems to split into two streams, one moving in a straight vertical path and the other stream moving in a wavy pattern. Observation of the dye streams from the top of the cell indicated that the first stream was very close to the wall, perhaps in the viscous sublayer, and the second dye stream was further from the wall, about 1 mm and probably in the outer part of the boundary layer undergoing transition, thus explaining the waviness.

The flow visualization results indicate that the inactive core does not play an important role in transferring heat from the heated walls to the cooled walls. The heat transfer is accomplished almost entirely by flow in the boundary layers up the heated walls, across the top, and down the cooled walls. One would then expect that heat transfer results would not be very sensitive to which walls are heated and which walls are cooled. This is borne out by the measurements of the heat transfer coefficients for each wall. For example, the three cold walls in the configuration CHCC have approximately equal heat transfer coefficients, likewise, the three hot walls in the configuration HHHC have approximately equal heat transfer coefficients.

Initially, the heat transfer coefficients were calculated using the overall temperature differences ΔT_o. This yielded a larger Nu (at fixed Ra) for a single wall of given temperature in a configuration with three walls of given temperature, e.g., the hot wall in CHCC had a Nu about three times that for the cold walls. Since flow visualization studies showed that the flow is essentially a boundary-layer flow that must be driven by the temperature difference between the wall and the core, it seemed more appropriate to use that temperature difference to derive the heat transfer coefficient. The core temperature was taken to be the bulk temperature, T_b, the average of the four wall temperatures.

Results for the configuration HHCC are shown in Fig. 7. The four points at each Ra represent the Nu for each of the four walls. The difference in Nu for a given Ra for the walls is quite small so the same symbol has been plotted in the figure for all four points. Some fine detail is revealed for each wall and for each configuration, although the correlation is obviously of the form $Nu \sim Ra^m$. For example, in the configuration HHHC, the Nu at $Ra > 10^{10}$ tends to lie above a correlation line passed through the higher Ra points by about 12 percent. Since the core flow could weakly influence the boundary layer flow, it is possible that this was due to the observed change in the core flow pattern as Ra was increased beyond 10^{10} as discussed in the first part of this section. These

details produce only minor variations in the Nu from an expected value (from a correlation equation for example) and should be the subject of further study.

For developing a useful correlation of reasonable accuracy, data points for all walls and all configurations (416 data points) are plotted in Fig. 8. A regression analysis gave the correlation

$$\mathrm{Nu} = 0.620\ \mathrm{Ra}^{0.250} \tag{3}$$

for $0.3 < \mathrm{Ra} < 6 \times 10^{10}$. The standard deviation from this correlation equation is ±5.7 percent. Notwithstanding the transition to turbulence at the higher Ra as evidenced by flow visualization, the Nu data correlate well with a 1/4 power of Ra as predicted from laminar boundary layer theory. The power of the Ra in equation (3) was calculated from the regression analysis and is not an assumed value of 1/4. This further confirms that the heat transfer mechanism is laminar convection in the boundary layers along vertical walls surrounding the core region as observed by flow visualization and as previously discussed for two dimensional flow. Since transition occurs in a region where the local heat transfer coefficient is significantly less than the average value (due to a smaller local temperature gradient from the wall to the stratified bulk fluid) as discussed in [23], the effect of transition on the average Nu is suppressed. The $\mathrm{Ra}^{1/4}$ dependence may be expected to hold until a substantial portion of the wall boundary layer is turbulent. Boundary layer waviness was observed in only the upper 1/3 of the hot wall for $\mathrm{Ra} > 3 \times 10^{10}$ in these experiments.

The leading constant in equation (3) is partially an artifact of the temperature difference used to calculate the heat transfer coefficient. The choice of wall-to-bulk temperature difference collapses all results to one correlation curve, equation (3), because the heat transfer mechanism is boundary layer convection, and as demonstrated by the flow visualization experiment, the boundary layer flow is not disturbed by the presence of adjacent walls and is thus configuration independent, at least for aspect ratios near one. Numerical results [23] show that the variation in heat transfer across the wall in the horizontal direction is negligible. This choice of temperature difference, however, requires some care when making comparison with previous work. If previous two-dimensional analyses and experiments has been based on the wall-to-bulk temperature rather than the overall temperature difference, the coefficient of the Rayleigh number would double (since the bulk temperature is the average of hot and cold wall temperatures). From the discussion presented in the Introduction, most of the analyses and experiments would then yield $\mathrm{Nu} = (.6 \text{ to } .8)\ \mathrm{Ra}^{1/4}$. For comparison purposes, we have plotted in Fig. 1 Nu/2 for the present three-dimensional work, i.e., $\mathrm{Nu} = 0.310\ \mathrm{Ra}^{0.250}$, and that the comparison can be seen to be quite favorable with the two-dimensional analyses and experiments (see Fig. 1). It should also be noted that the experimental ($A = 0.5$) data of [27] and [29] are slightly higher than the present results, as predicted by numerical results of [13] and [14].

Conclusions

Flow visualization experiments and heat transfer measurements have been completed for three-dimensional natural convection in a cubical enclosure at high Rayleigh number, $0(10^{10})$. The test cell has an adiabatic top and bottom and isothermal vertical walls. Four combinations of heating and cooling the isothermal walls were tested.

The flow visualization experiments verified the existence of a relatively inactive core surrounded by boundary layers on each of the four vertical walls. Transport of heat from the heated walls to the cooled walls is carried out by flow in the boundary layers. Relatively cool fluid near the bottom of the heated wall flows vertically up the heated wall absorbing heat from the wall. The boundary layer turns the corner at the cell top, and the heated fluid moves across the top to the cooled wall where the heat is given up in the reverse process. Boundary layers were observed to be essentially two-dimensional, i.e., they were not affected by the presence of nearby perpendicular walls.

Transition to turbulence was observed near the top 1/3 of the heated walls and near the bottom 1/3 of the cooled walls for the higher Ra. A waviness in the boundary layer consisting essentially of a single wavelength propagated along the wall until breaking near the top (bottom) of the heated (cooled) wall. The waves observed in the boundary layer were essentially two-dimensional, i.e., they extended across the wall from one edge to the other in a horizontal line.

Heat transfer measurements consist of average heat transfer coefficients for each wall and for each of four configurations of heated wall and cooled walls. The Ra was varied from about 0.3 to 6×10^{10}, and the Prandtl number was in the range of 3.5 to 6.0. Data were plotted in the form of Nu versus Ra on a log-log plot to reveal a straight line relationship. When heat transfer coefficients were based on the wall-to-bulk temperature difference, data for all walls and for all configurations collapsed to a single correlation equation, which agrees quite favorably with analyses and experiments in two-dimensional enclosures. The heat transfer mechanism is convection in the boundary layers that are not affected by the different core flows set up for the different configurations. The correlation indicates a laminar boundary-layer flow heat transfer mechanism, even though transition to turbulence was observed in the higher Ra experiments.

References

1 Batchelor, G. K., "Heat Transfer by Free Convection Across a Closed Cavity Between Vertical Boundaries at Different Temperatures," *Quarterly of Applied Mathematics*, Vol. 12, 1954, pp. 209-233.

2 Eckert, E. R. G., and Carlson, W. D., "Natural Convection in an Air Layer Enclosed Between Two Vertical Plates With Different Temperatures," *International Journal of Heat and Mass Transfer*, Vol. 2, 1961, pp. 106-120.

3 Elder, J. W., "Laminar Free Convection in a Vertical Slot," *Journal of Fluid Mechanics*, Vol. 23, 1965, pp. 77-98.

4 Elder, J. W., "Turbulent Free Convection in a Vertical Slot," *Journal of Fluid Mechanics*, Vol. 23, 1965, pp. 99-111.

5 Gill, A. E., "The Boundary-Layer Regime for Convection in a Rectangular Cavity," *Journal of Fluid Mechanics*, Vol. 26, 1966, pp. 515-536.

6 Bejan, A., "Note on Gill's Solution for Free Convection in a Vertical Enclosure," *Journal of Fluid Mechanics*, Vol. 90, 1979, pp. 561-568.

7 Simpkins, P. G., and Dudderar, T. D., "Convection in Rectangular Cavities with Differentially Heated End Walls," *Journal of Fluid Mechanics*, Vol. 110, 1981, pp. 433-456.

8 Raithby, G. D., and Hollands, K. G. T., "A General Method of Obtaining Approximate Solutions for Laminar and Turbulent Free Convection Problems," *Advances in Heat Transfer*, Academic Press, Vol. 11, 1975, pp. 265-315.

9 Raithby, G. D., Hollands, K. G. T., and Unny, T. E., "Analysis of Heat Transfer by Natural Convection Across Vertical Fluid Layers," ASME JOURNAL OF HEAT TRANSFER, Vol. 99, 1977, pp. 287-293.

10 Emery, A., and Chu, N. C., "Heat Transfer Across Vertical Layers," ASME JOURNAL OF HEAT TRANSFER, Vol. 87, 1965, pp. 110-116.

11 Newell, M. E., and Schmidt, F. W., "Heat Transfer by Laminar Natural Convection Within Rectangular Enclosures," ASME JOURNAL OF HEAT TRANSFER, Vol. 92, 1970, pp. 159-165.

12 Boyack, B. E., and Kearney, D. W., "Heat Transfer by Laminar Natural Convection in Low Aspect Ratio Cavities," ASME Paper No. 72-HT-52, 1972.

13 Inaba, H., Seki, N., Fukusako, S., and Kanayama, K., "Natural Convective Heat Transfer in a Shallow Rectangular Cavity With Different End Temperatures," *Numerical Heat Transfer*, Vol. 4, 1981, pp. 459-468.

14 Strada, M., and Heinrich, J. C., "Heat Transfer in Natural Convection at High Rayleigh Numbers in Rectangular Enclosures: A Numerical Study," *Numerical Heat Transfer*, Vol. 5, 1982, pp. 81-93.

15 Bejan, A., "A Synthesis of Analytical Results for Natural Convection Heat Transfer Across Rectangular Enclosures," *International Journal of Heat and Mass Transfer*, Vol. 23, 1980, pp. 723-726.

16 MacGregor, R. K., and Emery, A. F., "Free Convection Through

Vertical Plane Layers—Moderate and High Prandtl Number Fluids," ASME JOURNAL OF HEAT TRANSFER, Vol. 91, 1969, pp. 391–403.

17 Dropkin, D., and Somerscales, E., "Heat Transfer by Natural Convection in Liquids Confined by Two Parallel Plates Which are Inclined at Various Angles with Respect to the Horizontal," ASME JOURNAL OF HEAT TRANSFER, Vol. 87, 1965, pp. 77–84.

18 Burnay, G., Hannay, J., and Portier, J., "Experimental Study of Free Convection in a Square Cavity," *Heat Transfer and Turbulent Buoyant Convection*, Vol. II, edited by D. B. Spalding and N. Afgan, Hemisphere Publishing, 1977, pp. 807–811.

19 ElSherbiny, S. M., Raithby, G. D., and Hollands, K. G. T., "Heat Transfer by Natural Convection Across Vertical and Inclined Air Layers," ASME JOURNAL OF HEAT TRANSFER, Vol. 104, 1982, pp. 96–102.

20 Bejan, A., and Tien, C. L., "Laminar Natural Convection Heat Transfer in a Horizontal Cavity With Different End Temperatures," ASME JOURNAL OF HEAT TRANSFER, Vol. 100, 1978, pp. 641–647.

21 Shiralkar, G., Gadgil, A., and Tien, C. L., "High Rayleigh Number Convection in Shallow Enclosures With Different End Temperatures," *International Journal of Heat and Mass Transfer*, Vol. 24, 1981, pp. 1621–1629.

22 Tichy, J., and Gadgil, A., "High Rayleigh Number Laminar Convection in Low Aspect Ratio Enclosures With Adiabatic Horizontal Walls and Differentially Heated Vertical Walls," ASME JOURNAL OF HEAT TRANSFER, Vol. 104, 1982, pp. 103–110.

23 Gadgil, A., "On Convective Heat Transfer in Building Energy Analysis," Ph.D. thesis, Department of Physics, University of California, Berkeley 1979; also LBL-10900, Lawrence Berkeley Laboratory Report.

24 Imberger, J., "Natural Convection in a Shallow Cavity With Differentially Heated End Walls. Part 3. Experimental Results," *Journal of Fluid Mechanics*, Vol. 65, 1974, pp. 247–260.

25 Bejan, A., Al-Homoud, A. A., and Imberger, J., "Experimental Study of High Rayleigh-Number Convection in a Horizontal Cavity With Different End Temperatures," *Journal of Fluid Mechanics*, Vol. 109, 1981, pp. 283–299.

26 Sernas, V., and Lee, E. I., "Heat Transfer in Air Enclosures of Aspect Ratio Less than One," ASME JOURNAL OF HEAT TRANSFER, Vol. 103, 1981, pp. 617–622.

27 Bauman, F., Gadgil, A., Kammerud, R., and Greif, R., "Buoyancy-Driven Convection in Rectangular Enclosures: Experimental Results and Numerical Calculations," ASME Paper No. 80-HT-66, 1980.

28 Gadgil, A., Bauman, F., and Kammerud, R., "Natural Convection in Passive Solar Buildings: Experiments, Analysis, and Results," *Passive Solar Journal*, Vol. 1, 1982, pp. 28–40.

29 Nansteel, M., and Greif, R., "Natural Convection in Undivided and Partially Divided Rectangular Enclosures," ASME JOURNAL OF HEAT TRANSFER, Vol. 103, 1981, pp. 623–629.

30 Mallinson, G. D., and deVahl Davis, G., "Three-Dimensional Natural Convection in a Box: A Numerical Study," *Journal of Fluid Mechanics*, Vol. 83, 1977, pp. 1–31.

31 Hjertager, B. H., and Magnussen, B. F., "Numerical Prediction of Three-Dimensional Turbulent Buoyant Flow in a Ventilated Room," *Heat Transfer and Turbulent Buoyant Convection*, Vol. II, edited by D. B. Spalding and N. Afgan, Hemisphere Publishing, 1977, pp. 429–441.

32 Morrison, G. L., and Tran, V. Q., "Laminar Flow Structure in Vertical Free Convective Cavities," *International Journal of Heat and Mass Transfer*, Vol. 21, 1978, pp. 203–213.

33 Hieber, C., and Gebhart, B., "Stability of Vertical Natural Convection Boundary Layers: Some Numerical Solutions" *Journal of Fluid Mechanics*, Vol. 48, 1971, pp. 625–646.

34 Gebhart, B., *Heat Transfer*, ch. 8, 2d ed., McGraw-Hill, New York, 1971.